Sensors & Transducers, Vol. 24, Special Issue, August 2013, pp. 19-27

www.sensorsportal.com

Sensors & Transducers

http://www.sensorsportal.com

Impact of Environmental Vibration on Inertial Sensors' Output

[1] Jan ROHÁČ, [2] Stanislav ĎAĎO

Department of Measurement,
Faculty of Electrical Engineering, Czech Technical University in Prague
Technicka 2, 166 27 Prague, Czech Republic
Tel.: [1] +420 2 24353963, [2] +420 2 24352132, fax: +420 2 33339929
E-mail: xrohac@fel.cvut.cz, dado@fel.cvut.cz

Received: 15 May 2013 /Accepted: 16 August 2013 /Published: 30 August 2013

Abstract: The paper is dealing with an environmental strong-vibration impact on inertial sensors' output. In our case we measured data on the ultra-light aircraft ATEC 321, which did not have damped cockpit panel, and we recorded the data for post-processing. The main contribution of this paper is in frequency spectrum analyses of measured data, their validation, and filtering to ensure acceptable behavior of navigation systems relying on these data. The data suffered from strong vibration, which had big impact and thus it had to be removed before estimation of navigation parameters was performed. One example of navigation systems is an artificial horizon. Generally, it performs the aircraft attitude estimation just based on accelerometers and angular rate sensors data, and therefore the correctness and efficiency of data filtering as well as consecutive data processing plays a key role. *Copyright © 2013 IFSA.*

Keywords: Data processing, Wavelet multi-resolution filter, Angular rate sensors, Accelerometers.

1. Introduction

This paper extends the scope of previously published paper [1] concerning applicability of wavelet multi-resolution filters to reduce strong vibration impact on inertial sensors' data and their processing in aircraft navigation systems. The extension deals with methods how to validate data before their processing, with detailed description of different types of the mother wavelets and their comparison from their data filtering performances point of view.

1.1. Inertial Sensors' Data Processing

Due to the rapid proliferation of low-cost inertial sensors based on MEMS (Micro-Electro-Mechanical Sensors) technology in recent years, it has become viable to construct inexpensive strap down navigation systems. These systems can be used in many areas of research, especially where autonomous navigation is required. This includes unmanned vehicle systems and automotive as well as airborne applications, where estimation of attitude and/or displacement information is realized using various data fusion methods, for example a complementary filtering [2]. An artificial horizon is a typical example of these applications. It is a navigation system that belongs to the group of mandatory equipment required for each aircraft based on the regulations of aviation authorities. The system primarily displays aircraft orientation in space, which is described by a bank and elevation angle [3]. Estimation of these angles is based on angular rate measurements along the main aircraft

axes [4]. Originally, electro-mechanical gyroscopes were used on board large aircrafts; however, these have been replaced by laser gyros in most cases by now. Laser gyros are very expensive for their usage on small and ultra-light aircrafts, and therefore low-cost MEMS angular rate sensors are a suitable alternative. These sensors have numerous advantages such as small size, weight, price, and power consumption. On the other hand, they suffer from high drift rate, low sensitivity etc., which cause serious drawbacks that have to be dealt with. Because of these characteristics and the fact that an aircraft attitude is estimated by angular rate integration, a stand-alone solution with MEMS angular rate sensors cannot be realized. Integration in the estimation process causes unbound error growth due to noise and, especially, presence of vibrations in the measured data [5, 6]. So it is very useful to use accelerometers to provide the attitude correction under conditions when only a gravitational acceleration is applied to accelerometers, which is an ideal case. Generally, accelerometers are affected by combination of several accelerations, among which the vibrations dominate.

1.2. Environment Characterization

Even if the system is under laboratory conditions, the filtering of sensor outputs is obligatory because of the sensors' noise, which increases inaccuracy after angular rate integration. An additional aspect of inaccuracy is caused by environmental vibrations. In our case we used Inertial Measurement Unit (IMU) ADIS16350 from Analog Devices and measured angular rates and acceleration during all stages of flight such as parking, rolling on a runway, taking off, flying, and landing. The IMU was utilized in EFIS INTEGRA TL-6524 system manufactured by TL-Elektronic Inc. and mounted in the instrument panel of ATEC 321, see Fig. 1.

Data suffered from strong vibration which was also caused by the fact that the instrument panel of ATEC 321 was not equipped with vibration dampers. The sampling frequency was 43 Hz. A vibration character can be seen in Fig. 2 and Fig. 3. Parts (a) of these figures present time series of accelerations and angular rates measured in all axes during the parking and parts (b) correspond to their frequency spectrum.

(a) (b)

Fig. 1. ATEC 321 aircraft (a), EFIS INTEGRA TL-6524 (b).

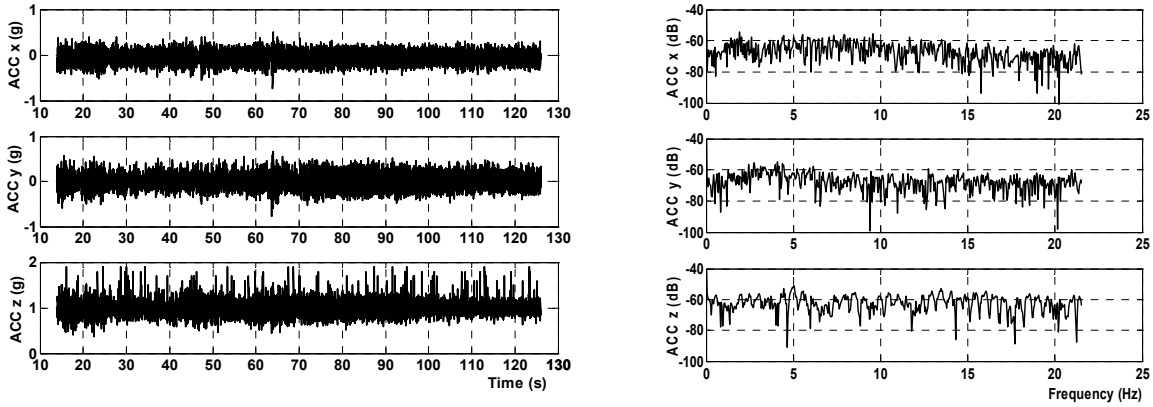

(a) (b)

Fig. 2. Acceleration measured during parking with the engine on, time series (a), FFT analysis (b).

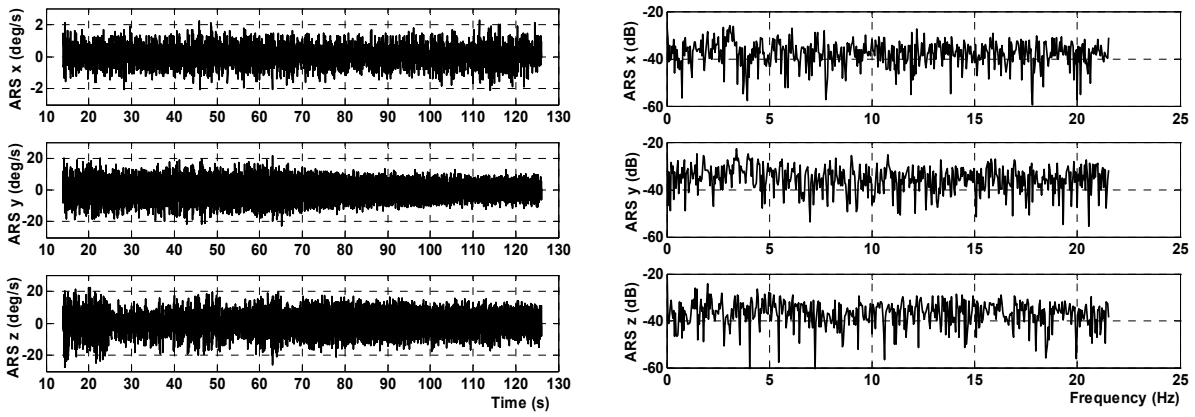

(a) (b)

Fig. 3. Angular rates measured during parking with the engine on, time series (a), FFT analysis (b).

Based on FFT analyses it can be seen that the frequency spectrum of vibrations is almost flat; nevertheless, according to Fig. 2 and Fig. 3 the vibration has higher impact during the parking in the range of (3 up to 10) Hz. When the aircraft is in the air the frequency range changes according to flight conditions, mostly going up. In cases of engine RPM (Revolution per Minute) suppression during the flight, vibration frequencies go down all the way to 0.5 Hz, as shown in Fig. 4 and Fig. 5. The vibration has similar character in all axes except the z-axis in ACC and x-axis in ARS measurements. It is caused by a natural wing damping feature.

2. Data Characterization

2.1. Validation of Sensor Data

Vibration could damage the sensor or at least influence its transfer function. From this reason it is advisable to include the diagnostic procedure for checking the consistency of sensor performance. One possibility is to use data validation process based on Probabilistic Data Association Filter (PDAF) [7] described schematically in block diagram of modified Kalman filter system on Fig. 6.

The sensors' output data **y** is compared with the values derived from state equation of system. The statistical parameters of innovation expression

$$\mathrm{n}(t) = \mathrm{y}(t) - \hat{\mathrm{y}}(t \mid t-1) = \mathrm{y}(t) - \mathrm{C}\hat{\mathrm{x}}(t \mid t-1), \quad (1)$$

are examined in a validation gate. The examination process consists in the determination of statistical (Mahalonobis) distance given by the expression

$$d^2(t) = \mathbf{n}(t).\mathbf{S}(t).\mathbf{n}^T(t), \quad (2)$$

where $S(t)$ is related to an estimated covariance matrix P and a measurement noise matrix R as follows

$$S(t) = CP(t,t-1)C^T + R. \quad (3)$$

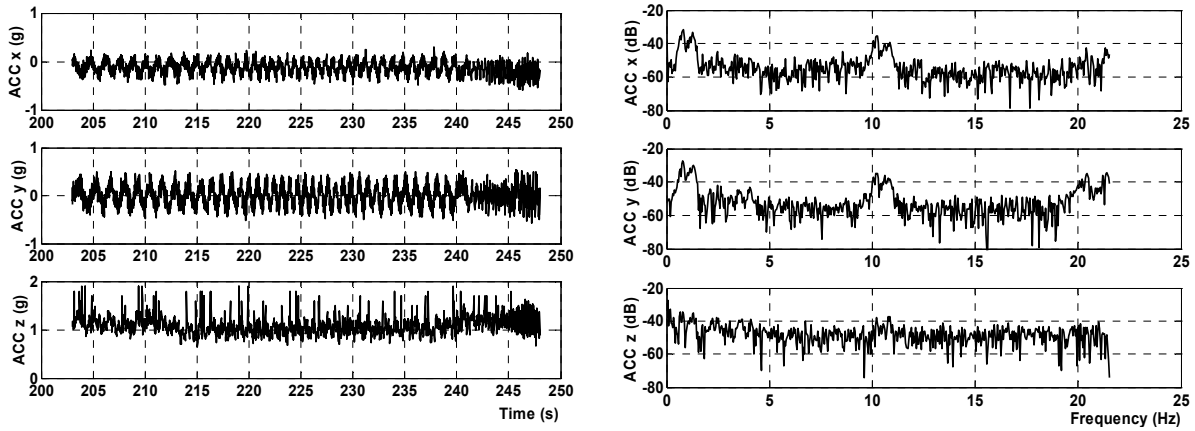

(a) (b)

Fig. 4. Acceleration measured during engine RPM suppression, time series (a), FFT analysis (b).

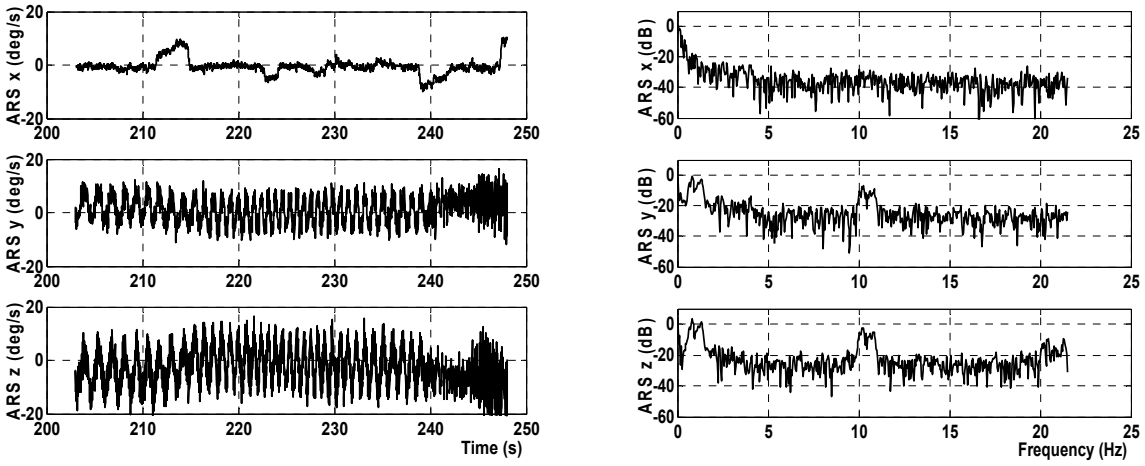

(a) (b)

Fig. 5. Angular rates measured during engine RPM suppression, time series (a), FFT analysis (b).

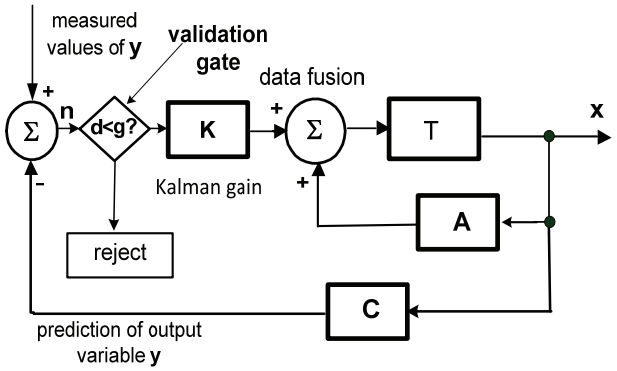

Fig. 6. Principle of the Kalman filter data validation by a PDAF method. (***A***, ***C*** correspond to a state and measurement system model matrices, ***x*** is a state vector, ***y*** denotes a measurement vector, ***K*** is a Kalman gain, and ***T*** represents a delay).

When there is satisfied the condition

$$d^2(t) \le g \tag{4}$$

newly measured values **y** is used for a new a-posteriori state estimation. In the opposite case, the inconsistent data are excluded and previously estimated $\hat{x}$ is used. Moreover, the data on rejection output of validation gate are used for diagnostic purposes.

2.2. Characterization of Vibrations Causing Errors by Allan Variance

The effect of vibrations on sensor performance could also be evaluated using Allan variance approach. In terms of Allan variance harmonic components of mechanical vibrations affecting sensor could act as sinusoidal type of noise [8]. Power spectral density (PSD) of this noise can be characterized by a number of distinct frequencies. The PSD of noise containing a single frequency f_0 and amplitude Ω_0 is given by sum of Dirac δ−functions

$$S_\Omega(f) = \frac{1}{2}\Omega_0^2\left[\delta(f - f_0) + \delta(f + f_0)\right]. \tag{5}$$

In the case of multiple frequencies f_{0i} of the sinusoidal errors it can be similarly represented by a sum of Dirac δ-functions. As it is well known the procedure of finding Allan variance is equivalent to filtering a noise PSD by a filter with a transfer characteristic

$$H(f) = \frac{\sin^4(\pi f\tau)}{(\pi f\tau)^2}. \tag{6}$$

The Allan variance can then be found by performing integration

$$\sigma^2(\tau) = 4\int_0^\infty S_\Omega(f).H(f)df = \Omega_0^2\left(\frac{\sin^2 \pi f_0\tau}{\pi f_0\tau}\right)^2 \tag{7}$$

Log-log plot of root Allan variance, according to [8], is composed from several peaks with amplitudes falling off rapidly as shown in Fig. 7. Estimation of a sinusoidal noise from sensor data might be complicated as it requires the observation of several peaks. Moreover, the peaks due to a sinusoidal noise could be masked by higher order peaks of other frequencies. This fact makes the estimation of error bounds difficult and further justifies the proposed filtering approach to minimization of sinusoidal errors' influences.

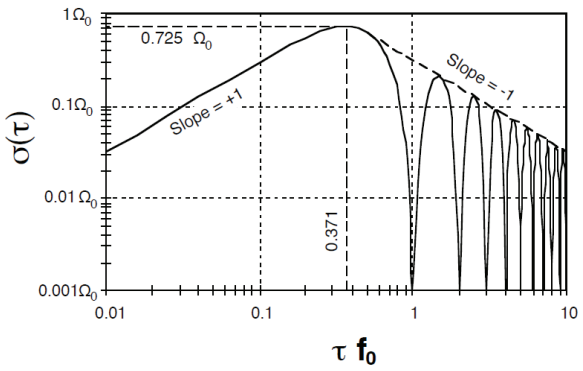

Fig. 7. Square root of Allan Variance plot for a sinusoidal error [8].

3. Wavelet Multi-Resolution Filter

3.1. Digital Filters

To reach sufficient results and to smooth inertial signals efficiently we analyzed in [1] different filtering approaches with filters FIR, IIR, MA (Moving Average), and windowed-sinc filters. We suggested the solution using two different filter approaches for accelerometers' and angular rate sensors' data. According to results obtained from FFT analyses a main problem is that a vibration bandwidth and aircraft dynamics overlap and thus the separation of a useful signal from the unwanted one caused by the vibration cannot be done. Therefore, it is required for correct attitude estimation to remove only high frequency noise from angular rate data by low-order low-pass filter, which would respect the aircraft dynamic bandwidth. Nevertheless, in the case of accelerometers the situation is different. It is not required to respect the aircraft dynamics, so it is possible to use high-order low-pass filter with a cut-off frequency set to a level in which a vibration impact can be removed. Its main goal is to restrict the vibration impact on very low frequencies, in our case down to 0.5 Hz. For this reason we had to search for a filter fulfilling requirements on system stability even at such low frequencies. Above mentioned filters did not satisfy these requirements, for details see [1], and thus we searched for other possibility which we found in wavelet multi-resolution filter application. This provided as smooth data as possible with an acceptable time delay which was dealt with in a data fusion process.

Even if the aircraft ATEC321 is light and well maneuverable, we considered flight dynamics bandwidth to 15 Hz and usage of first-order low-pass filter (LPF) for angular rates data. A continuous time transfer function of LPF is defined as

$$H(s) = \frac{y(s)}{u(s)} = \frac{1}{1 + s\tau}, \qquad (8)$$

where τ is a time constant, $y(s)$ denotes the Laplace transform of the filter output, and $u(s)$ corresponds to the input.

The time constant of the LPF is related to its cut-off frequency f_m defined as

$$f_m = \frac{1}{2\pi\tau}. \qquad (9)$$

A discrete form of the LPF can be derived from (8) using difference equation and can be written as

$$y(k) = (1-a)\,y(k-1) + a\,u(k), \qquad (10)$$

where parameter $a = \frac{T_S}{T_S + \tau}$, k denotes the count of time steps, T_s is a sampling period.

3.2. Principle of the WMRF

Wavelet multi-resolution filtering (WMRF) relies on discrete wavelet transform (DWT) using a finite number of wavelet points. In the case when the spectrum of a useful signal and the one of a noise are overlapped, the WMRF is less harmful to a useful signal than any linear type of other filters. It also has advantages over traditional Fourier methods in analyzing physical situations where the signal contains discontinuities and sharp spikes [9]. Generally, wavelet techniques are based on analyzing a signal through windowing process with variable window size [10]. They allow usage of narrow windows (i.e. short time of observation) in cases when high frequency information is needed and wide windows (i.e. long time of observation) if low frequency information is required [11]. The wavelet transformation can be applied on a discrete signal sequence to decompose it into lower and higher frequency components using predetermined wavelet function, its shifting and scaling coefficients, and the level of decomposition. The DWT definition can be derived from the Continuous Wavelet Transform (CWT) of a time domain signal *x(t)* as described in [10, 12 p. 84, 13] as

$$CWT(a,b) = \frac{1}{\sqrt{a}} \int_{-\infty}^{\infty} x(t) \Psi(\frac{t-b}{a}) dt \,, \quad (11)$$

where *a* and *b* correspond to the scaling and shifting parameter of the wavelet function *Ψ(t)*.

Scaling the wavelet means stretching or compressing it in the time domain. The smaller the scale, the more the wavelet is compressed. Vice versa, the larger the scale, the more is stretched instead. The lower values of wavelet scales (coefficient *a*), the more suitable the wavelet is for analysis of high frequency signal components referred to as the signal "details". On the other hand, higher values of wavelet scales allow the analysis of low frequency signal components referred to as the signal "approximations" [10], [12]. The actual integration over time, i.e. Eq. (4), gives the CWT coefficients corresponding to *a* and *b*. These coefficients are considered to be the measure of correlation between the used wavelet function and the signal itself for different values of the scales (coefficient *a*) and different time locations (coefficient *b*) of the wavelet. The wavelet function *Ψ(t)* is the basis function (or mother wavelet) and it requires to have following properties to ensure the integration (4) is finite: to be short and oscillatory having zero average value and rapid convergence to zero at both ends [12]. The DWT definition is hence as follows, assuming *x(n)* to be discrete time sequence [12 p. 85, 13].

$$\begin{aligned} C_{a,b} &= 2^{(-a/2)} \sum_n x(n) \Psi_{a,b}(n) = \\ &= 2^{(-a/2)} \sum_n x(n) \Psi(2^{-a} - b) \end{aligned} \,, \quad (12)$$

where $C_{a,b}$ represents DWT coefficients, $\Psi(n)$ denotes the wavelet derived from the mother one based on scaling and shifting coefficients *a*, *b*.

The decomposed signal is then reconstructed by applying an inverse DWT (IDWT) on its computed DWT coefficients $C_{a,b}$. It is done by passing the coefficients of selected approximation level through the IDWT low-pass filter and resetting the coefficients of all subsequent details to zero before passing them through the IDWT high-pass filters. The filtered discrete signal $x_f(n)$ can be obtained by

$$x_f(n) = \sum_a \sum_b C_{a,b} \Psi_{a,b}(n) \,. \quad (13)$$

3.3. Performance of the WMRF

The WMRF is mostly used for data post-processing; nevertheless, in [1] we proposed a solution suitable for real-time applications noted as RT WMRF. In our solution a utilized decomposition low-pass filter impulse response was derived from the Symlet 4 mother wavelet. Wavelets of the same kind might differ in number of points (samples) in which the shape of the wavelet and derived decomposition and reconstruction filters are exactly defined. In the case of Symlet 4 the impulse response had 8 points as it can be seen in Fig. 8, where also Symlet 8, Daubechies 4, and Daubechies 8 are shown for a comparison. To prove the efficiency of the Symlet mother wavelets (sym4, sym8, sym16, sym32) we ran the analysis in which a wide-band white noise was applied for filtering using WDEN Matlab function with the Level of Decomposition (LoD) equal to 8 and a soft universal 'sqrtwolog' threshold.

The results of this analysis are shown in Fig. 9. It can be said that the higher number of points of the mother wavelet, the smoother performance from the FFT analysis point of view is. A similar character of a FFT analysis was observed when Daubechies mother wavelets (db4, db8, db16, db32) were applied. Moreover, we compared performances and noise reduction efficiency among Symlet and Daubechies derived mother wavelets; results are denoted in Table 1. According to reached results it might seem that Symlet 32 is optimal for a usage due to its smooth frequency domain performance and the highest reduction efficiency, but the number of the mother wavelet points is too high. Therefore, Symlet 4 was utilized in RT WMRF due to its second best noise reduction capability.

Table 1. Comparison of WMRF results with different mother wavelets applied.

Mother wavelet	Standard deviation (-)	Mother wavelet	Standard deviation (-)	No. of the wavelet points
sym4	0.081	***db4***	0.084	8
sym8	0.086	***db8***	0.087	16
sym16	0.083	***db16***	0.090	32
sym32	0.077	***db32***	0.083	64

4. Results of RT WMRF Application

In [1] proposed RT WMRF utilized a normalized sym4 mother wavelet and a corresponding decomposition low-pass filter. In each Level of Decomposition (LoD) the filter impulse response was convolved with an applied signal or its approximation from a previous LoD. After the last decomposition the algorithm was making an average of the last convolution results. Because the filter impulse response was normalized, the reconstruction was not needed, which reduced a computation load.

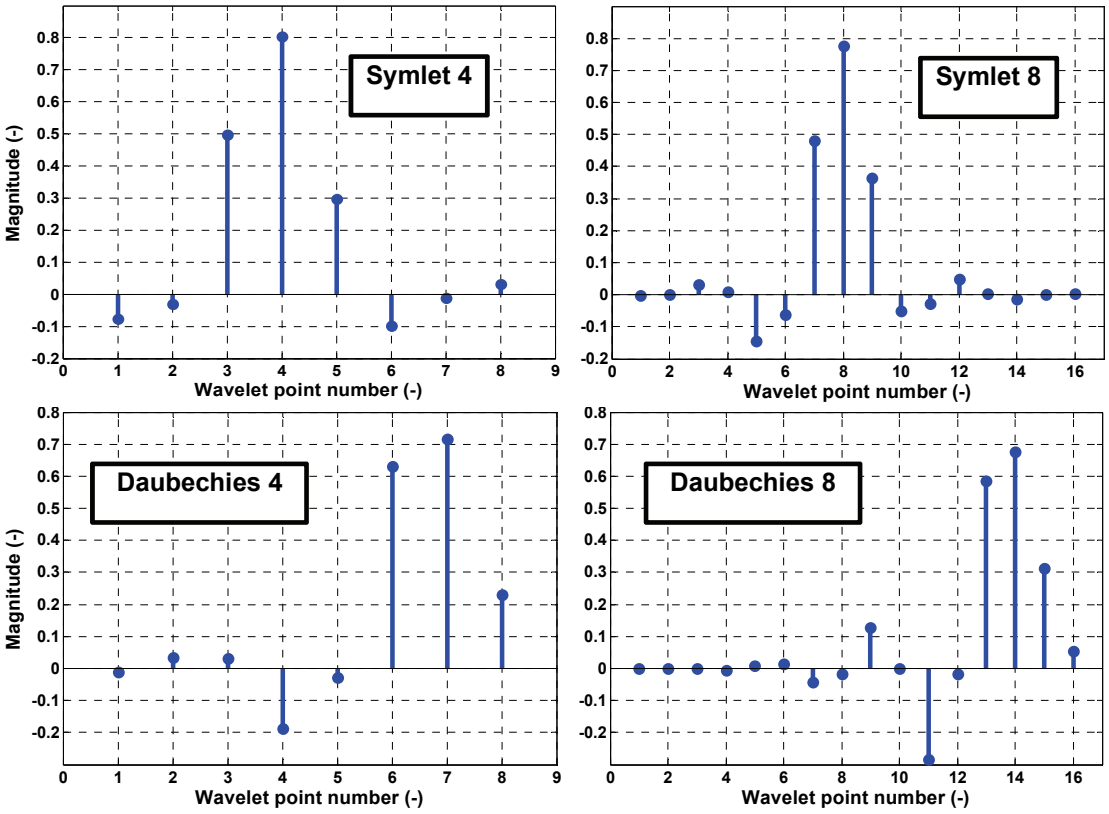

Fig. 8. Definition of discrete mother wavelet functions.

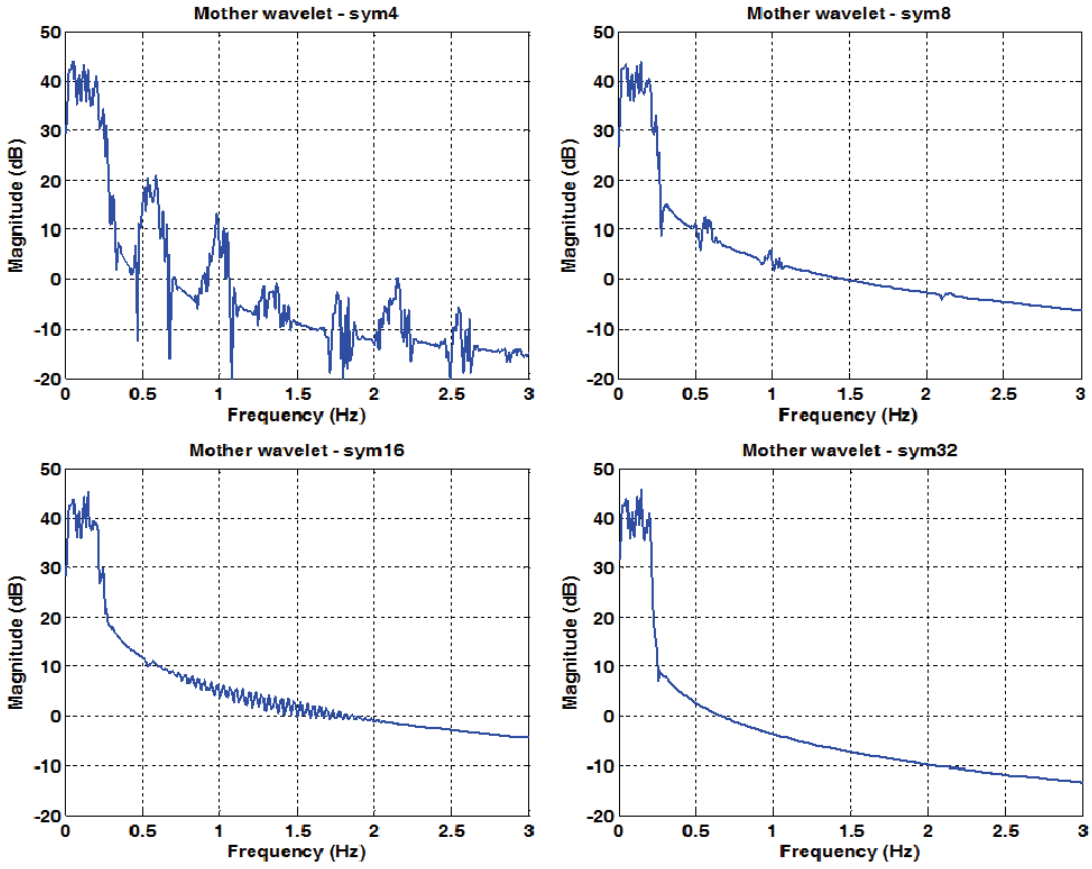

Fig. 9. FFT of WMRF with LoD=8, a soft universal 'sqrtwolog' threshold.

Results were compared to Matlab WDEN function also utilizing sym4 mother wavelet, the same level of decomposition, in this case equal to 8, and a soft universal 'sqrtwolog' threshold. The performances of both RT WMRF and WDEN function, when a white noise was applied as the input, are shown in Fig. 10.

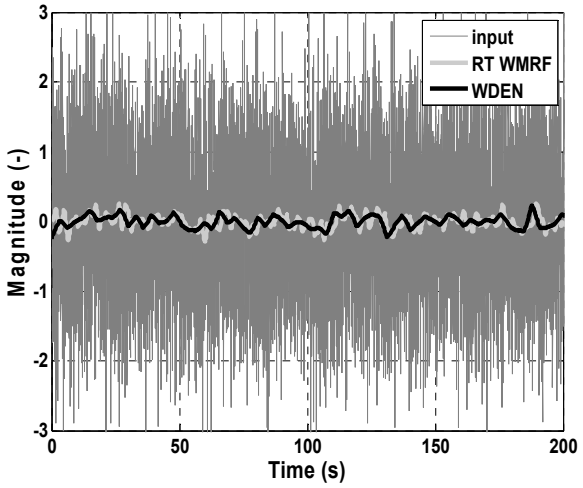

(a)

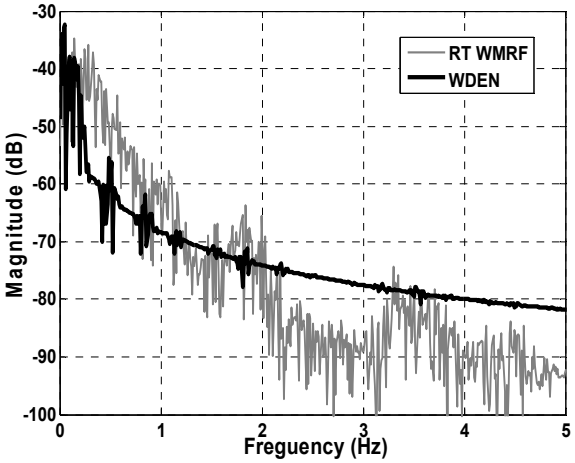

(b)

Fig. 10. Performance comparison of a proposed RT WMFR and WDEN function, time domain (a), frequency domain (b).

It can be seen in Fig. 10 that WDEN function is more efficient in low-frequency noise reduction due to a sharper edge on its frequency domain performance. Nevertheless, it should be considered that RT WMRF worked with a finite number of signal samples corresponding to 2^{LoD}, which is in contrast to WDEN function using the whole signal at once. In shown performances the LoD was set at 8, thus the number of samples used in RT WMRF was 256. The proposed RT WMRF provided stable solution and fulfilled adequate filtering capabilities required during all flight stages as shown in Fig. 11. Fig. 12 depicts zoomed tracks from Fig. 11 in different times so as to show different stages of flight. It confirms correct filter behavior even under strong low-frequency vibration conditions.

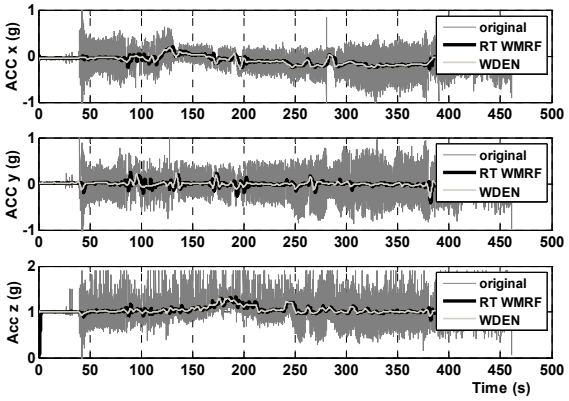

Fig. 11. RT WMRF applied on real flight data.

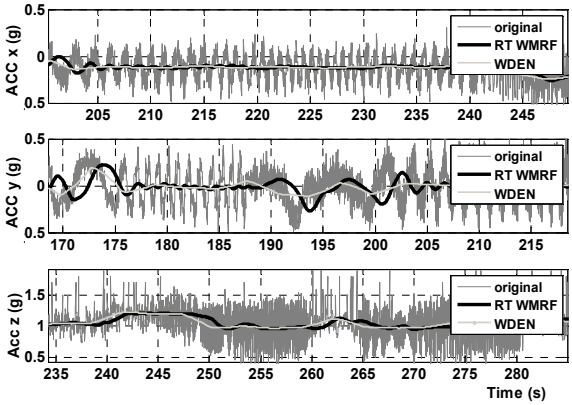

Fig. 12. RT WMRF applied on real flight data – zoomed tracks of Fig. 10.

5. Conclusions

This paper extends previously published results about in [1] proposed solution of a real-time WMRF (RT WMRF). This paper provides the frequency spectrum analyses of inertial sensors' data during different stages of flight and points out main problems for data evaluation. The main contribution is in the description of data validation process based on probabilistic data association filter and Allan variance analysis, and in detailed description of WMRF performances and their comparison. It was verified that the Symlet 4 as a mother wavelet applied in RT WMRF provided the best performance when the number of mother wavelet points and noise reduction efficiency was taken into account (the attenuation of components at

frequencies around 0.5 Hz is nearly 40 dB). Moreover, it was shown that RT WMRF had approximately a double bandwidth of WDEN function performance for the same level of decomposition. All is targeted at the application of RT WMRF proposed in [1] to prove its suitability to ensure required behavior of aircraft navigation systems relying on inertial sensors' data even in the case of strong vibration environment.

Acknowledgements

This research has been partially supported by the research program TA CR Alfa No. TA02011092 "Research and development of technologies for radiolocation mapping and navigation systems", and partially by Grant Agency of the Czech Technical University in Prague grant No.SGS10/288/OHK3/3T/13. Special thanks to TL elektronic Inc. for the aircraft and data provision.

References

[1]. J. Roháč, M. Reinštein, K. Draxler, Data processing of inertial sensors in strong-vibration environment, in *Proceedings of the 6th IEE International Conference on Intelligent Data Acquisition and Advanced Computing Systems (IDAACS'2011),* Prague, Czech Republic, 15-17 September 2011, Vol. 1, pp. 71-75.

[2]. V. Kubelka, M. Reinstein, Complementary filtering approach to orientation estimation using inertial sensors only, in *Proceedings of the IEEE International Conference on Robotics and Automation (ICRA' 2012)*, St. Paul, USA, 14-18 May 2012, pp. 599-605.

[3]. M. Sipos et al., Flight attitude track reconstruction using two AHRS units under laboratory conditions, in *Proceedings of the 8th IEEE Conference on Sensors*, Lecce, Italy, 26-29 October 2008, pp. 675-678.

[4]. D. H. Titterton, J. L. Weston, Strapdown inertial navigation technology, *Lavenham Press Ltd.*, Lavenham, UK, 1997.

[5]. P. G. Savage, Strapdown inertial navigation integration algorithm design, Part 1: Attitude algorithms, *Journal of Guidance, Control, and Dynamics*, Vol. 21, No. 1, 1998, pp. 19-28.

[6]. P. G. Savage, Strapdown inertial navigation integration algorithm design, Part 2: Velocity and position algorithms, *Journal of Guidance, Control, and Dynamics*, Vol. 21, No. 2, 1998, pp. 208-221.

[7]. A. M. Agogino, K. Goebel, S. Alag, Intelligent sensor validation and sensor fusion for reliability and safety enhancement in vehicle control, MOU132, Final Report, UCB-ITS-PRR-95-40, *California PATH Research Report*, 1995.

[8]. IEEE standard specification format guide and test procedure for single-axis interferometric fiber optic gyros, *IEEE Std 952™-1997 (R2008)*, [PDF] New York, USA 1997.

[9]. M. Sotak, R. Breda, Removing the high frequency noise components from gyro and accelerometer measurements, *Acta Avionica,* Vol. 10, No. 15, 2008, pp. 36-40.

[10]. S. Nassar, Improving the inertial navigation system (INS) error model for INS and INS/DGPS applications, PhD Thesis, Calgary, Canada, Department of Geomatics Engineering, *University of Calgary*, 2003. Vol. UCEG Reports Number 20183.

[11]. M. Sotak, Application of wavelet analysis to inertial measurements, *Science & Military,* Vol. 3, No. 2, 2008, pp. 17-20.

[12]. W. Abdel-Hamid, Accuracy enhancement of integrated MEMS-IMU/GPS systems for land vehicular navigation applications, PhD Thesis, Calgary, Canada: Department of Geomatics Engineering, *University of Calgary*, 2005, UCEG Reports Number 20207.

[13]. A. D. Poularikas, The handbook of formulas and tables for signal processing, USA, *CRC Press,* 1999.
